Application Limits of the Airgap Maxwell Tensor

Raphaël Pile, Guillaume Parent, Emile Devillers, Thomas Henneron, Yvonnick Le Menach, Jean Le Besnerais, Jean-Philippe Lecointe

Application Limits of the Airgap Maxwell Tensor

Raphaël Pile[1,2], Guillaume Parent[3], Emile Devillers[1,2], Thomas Henneron[2],
Yvonnick Le Menach[2], Jean Le Besnerais[1], and Jean-Philippe Lecointe[3]
[1]EOMYS ENGINEERING, Lille-Hellemmes 59260, France
[2]Univ. Lille, Arts et Metiers ParisTech, Centrale Lille, HEI, EA 2697 - L2EP -
Laboratoire d'Electrotechnique et d'Electronique de Puissance, F-59000 Lille, France
[3]Univ. Artois, EA 4025, Laboratoire Systèmes Électrotechniques et Environnement (LSEE), F-62400 Béthune, France

Airgap Maxwell tensor is widely used in numerical simulations to accurately compute global magnetic forces and torque but also to estimate magnetic surface force waves, for instance when evaluating magnetic stress harmonics responsible for electromagnetic vibrations and acoustic noise in electrical machines. This article shows that airgap surface forces based on Maxwell tensor with a circular contour depend on the radius of application. The dependence of surface forces on radius is analytically explained using an academic case of a slotless electric machine. The corrective coefficients that should be applied to transfer the airgap surface forces to stator (or rotor) bore radius are presented. The coefficients depend on the airgap geometry and surface forces wavenumber. The use of transfer coefficients is recommended to quantify the deviation due to the radius of application in the airgap. In addition, the transfer coefficients could be applied to correct the radial surface force component on the tip of the teeth assuming infinite permeability.

***Index Terms*—Maxwell tensor, Magnetic stress, Electrical machines, Magneto-mechanical, Vibroacoustic.**

I. Introduction

MAXWELL tensor (MT) is used to accurately compute overall forces on a given body. In particular, electrical machines designers are used to apply MT technique in the middle of the airgap to calculate the electromagnetic torque experienced by the rotor. This technique has been naturally extended to the study of magnetic force waves experienced by the outer structure - generally the stator - for vibroacoustic analysis. The method is generally based on a circular path in the airgap to ease physical interpretations with the Fourier transform [1,2]. In that case, one may look for a circular path as close as possible from the stator bore radius to accurately estimate forces experienced by the stator. Indeed, for magnetic linear media [3], the theoretical magnetic surface force density at the air-ferromagnetic interface is exactly given by MT expression.

However, the radius of the circular path has a strong influence on calculated stress harmonics [4]–[6]. In Finite Element Analysis (FEA) simulations, the mesh is generally the finest in the airgap so that it is recommended to evaluate forces in the middle of the airgap. Besides, 2D FEA based on scalar potential cannot ensure high accuracy of both radial and tangential flux density at the air-ferromagnetic interface, which are both involved in MT expression. Then the numerical application of the MT at the interface is source of numerical errors [5].

Therefore, it is interesting to know how to transfer surface forces based on MT calculated in the airgap to another radius, in particular at tooth tip radius. Such a transformation would also be useful when using analytical electromagnetic models such as permeance magneto-motive force models, which focus on the accurate calculation of the flux density distribution at the airgap radius.

Therefore, this article compares the deviation between the application of airgap surface force based on MT and the surface forces at stator bore radius. Due to numerous numerical artifacts in practical electrical machines, only a slotless stator and rotor with constant permeability is studied in this article. It allows to obtain the analytic expression of the airgap potential and resulting surface forces at any radius. Thus the surface force transfer deviation is quantified by analytically-derived transfer coefficients (20) and (24) which depend on airgap geometry and magnetic surface force wavenumber.

II. Problem definition

A. Maxwell Tensor

According to [3,7], for an incompressible linearly magnetizable media the magnetic flux density $\mathbf{B}$ is related to the magnetic field $\mathbf{H}$ $\forall \mathbf{x} \in \Omega$ by $\mathbf{B}(\mathbf{x}) = \mu(\mathbf{x}, B)\mathbf{H}(\mathbf{x})$ such that the magnetic stress tensor reduces to the following form:

$$\mathbf{T}_{\mathrm{m}} = -\mu \frac{\mathbf{H} \cdot \mathbf{H}}{2} \mathbf{I} + \mu \mathbf{H}\mathbf{H} \tag{1}$$

with $\mathbf{I}$ the identity tensor. In particular, the Vacuum Maxwell stress tensor is obtained for $\mu = \mu_0$. The theoretic application of this magnetic stress tensor for the computation of magnetic surface force density $\mathbf{P}$ on a contour which exactly corresponds to the air-ferromagnetic interface (defined by its local normal vector $\mathbf{n}$) leads to [3,5]:

$$\mathbf{P} = \left(\frac{1}{2} \left(\frac{1}{\mu_0} - \frac{1}{\mu} \right) B_{\mathrm{n}}^2 - \frac{\mu_0 - \mu}{2} H_{\mathrm{t}}^2 \right) \mathbf{n} \tag{2}$$

where B_{n} and H_{t} are the magnetic flux density locally normal (resp. magnetic field locally tangential) to the interface.

B. Airgap Surface Force

One of the most used method to compute magnetic surface forces based on MT is to use Stoke's theorem [8] along a

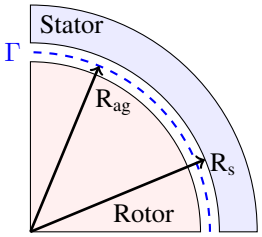

Fig. 1. Slotless electrical machine used to compare magnetic surface force on the stator and in the airgap

circular closed boundary Γ in the airgap at a given radius $\mathrm{R_{ag}}$ as illustrated in Fig 1. The result gives the total magnetic force $\mathbf{F}_\mathrm{m}$ acting on either the stator or rotor [1,5]:

$$\mathbf{F}_\mathrm{m} = \oint_\Gamma -\frac{\mu_0}{2} H^2 \mathbf{n} + \mu_0 H_\mathrm{n} \mathbf{H} \; d\Gamma \tag{3}$$

Then the airgap MT approximation is to assume the term under the integral to be the magnetic surface force density in the polar referential:

$$\begin{aligned} P_\mathrm{r}(\mathrm{R_{ag}}) &\approx \frac{1}{2\mu_0} B_\mathrm{r}(\mathrm{R_{ag}})^2 - \frac{\mu_0}{2} H_\theta(\mathrm{R_{ag}})^2 \\ P_\theta(\mathrm{R_{ag}}) &\approx B_\mathrm{r}(\mathrm{R_{ag}}) H_\theta(\mathrm{R_{ag}}) \end{aligned} \tag{4}$$

with P_r the radial magnetic surface force density, P_θ the tangential magnetic surface force density, B_r the radial magnetic flux density, and H_θ the tangential magnetic field. Neglecting the ferromagnetic permeability μ contribution into (2) gives an expression very similar to (4) justifying the use of airgap surface force approximation.

The application of (2) at the air-ferromagnetic interface remains source of numerical errors [5]: in the case of numerical model based on FEA, the continuity of both normal magnetic flux B_n density and tangential magnetic field H_t cannot be ensured on the interface between materials. As a consequence, publications often use airgap approximation (4) for the vibroacoustic design of electrical machines because the middle of the airgap is better meshed, it is less sensitive to variational formulation, and it allows the physical understanding of each magnetic force wave (for instance with analytical models) [1,2].

C. Studied Slotless Case

Understanding the sources of airgap surface force (4) variations is a difficult task because of numerous artifacts such as slotting effect, sharp geometries, interference between the wavenumbers, *etc*. To avoid these main artifacts, a specific case is defined:

- Slotless stator and rotor to avoid sharp geometries and slotting effect.
- Single-wave excitation to avoid interference between different wavenumbers.
- Analytical solving to avoid meshing and numerical errors.

The case presented in Fig. 1 proposes to fulfill all these constraints. The stator bore radius is $\mathrm{R_s}$ and the middle airgap radius is $\mathrm{R_{ag}}$. In order to have only one magnetic wavenumber, the magnetic potential z-component A_z is imposed at radius $\mathrm{R_{ag}}$ such that $\forall \theta \in [0, 2\pi]$:

$$A_\mathrm{z}(\mathrm{R_{ag}}, \theta) = \beta_n \sin(n\theta + \psi_n), \;\; n \in \mathbf{N}^* \tag{5}$$

The continuity of tangential magnetic field can be expressed with the magnetic potential at the interface between the air (permeability μ_0) and ferromagnetic media (permeability μ) $\forall \theta \in [0, 2\pi]$:

$$\frac{1}{\mu_0} \frac{\partial A_\mathrm{z}}{\partial r}(\mathrm{R_s^-}, \theta) = \frac{1}{\mu} \frac{\partial A_\mathrm{z}}{\partial r}(\mathrm{R_s^+}, \theta) \tag{6}$$

Thus the boundary condition at $r = \mathrm{R_s}$ with $\mu_\mathrm{r} \to \infty$ becomes:

$$\frac{\partial A_\mathrm{z}}{\partial r}(\mathrm{R_s}, \theta) = 0 \tag{7}$$

For these boundary conditions, Poisson's equation is solved for the 2D magnetic vector potential in polar coordinates $\forall \theta \in [0, 2\pi]$ and $\forall r \in [\mathrm{R_{ag}}, \mathrm{R_s}]$:

$$\frac{1}{r} \frac{\partial}{\partial r} \left(\frac{1}{r} \frac{\partial A_\mathrm{z}}{\partial r} \right) + \frac{\partial^2 A_\mathrm{z}}{\partial \theta^2} = 0 \tag{8}$$

This partial derivative problem can be solved analytically [9]. Thus the magnetic potential, flux density and field can be analytically computed in the studied domain. The next section provides the calculation steps which lead to the analytical expression of flux density (15) in the slotless case.

D. Analytic Magnetic Solving in Slotless Case

A solution exists and is unique for the previous system composed of (8), (7) and (5) according to [8]. Then a method consists in stating a function A_z and to check if it fulfills the boundary conditions: a solution similar to [9] is searched $\forall \theta \in [0, 2\pi]$ and $\forall r \in [\mathrm{R_{ag}}, \mathrm{R_s}]$:

$$A_\mathrm{z}(r, \theta) = \frac{\gamma_n E_n(r, \mathrm{R_s}) + \alpha_n E_n(\mathrm{R_{ag}}, r)}{E_n(\mathrm{R_{ag}}, \mathrm{R_s})} \sin(n\theta + \psi_n) \tag{9}$$

with E_n a polynomial function defined by:

$$E_n : (x, y) \in \mathbb{R}^2 \to (x/y)^n - (y/x)^n \tag{10}$$

Under this form, the vector A_z is satisfying Poisson's equation (8). Then the coefficient γ_n, α_n, have to be determined in order to satisfy the boundary conditions. If a correct set of these coefficients is found, then A_z would be the unique solution of the problem. First, satisfying the boundary condition (5) in the airgap leads to:

$$\gamma_n = \beta_n \tag{11}$$

The second boundary condition (7) leads to:

$$\alpha_n = 2\beta_n / F_n(\mathrm{R_{ag}}, \mathrm{R_s}) \tag{12}$$

with F_n a polynomial function defined by:

$$F_n : (x, y) \in \mathbb{R}^2 \to (x/y)^n + (y/x)^n \tag{13}$$

Thus, the unique solution of the system is entirely defined with the geometrical parameters and excitation's wavenumber. The flux density is derived from the magnetic potential:

$$\mathbf{B} = \mathbf{curl}(\mathbf{A}) = \frac{1}{r} \frac{\partial A_z}{\partial \theta} \mathbf{e}_\mathrm{r} - \frac{\partial A_z}{\partial r} \mathbf{e}_\theta = B_\mathrm{r} \mathbf{e}_\mathrm{r} + B_\theta \mathbf{e}_\theta \tag{14}$$

With (14) and (9) both radial and tangential magnetic flux can be analytically expressed for this slotless machine:

$$\begin{aligned} B_{\mathrm{r}}(r,\theta) &= \frac{n\beta_n}{r}\frac{E_n(r,\mathrm{R_s}) + \frac{2E_n(\mathrm{R_{ag}},r)}{F_n(\mathrm{R_{ag}},\mathrm{R_s})}}{E_n(\mathrm{R_{ag}},\mathrm{R_s})}\cos(n\theta+\psi_n) \\ B_{\theta}(r,\theta) &= -\frac{n\beta_n}{r}\frac{F_n(r,\mathrm{R_s}) + \frac{2F_n(\mathrm{R_{ag}},r)}{F_n(\mathrm{R_{ag}},\mathrm{R_s})}}{E_n(\mathrm{R_{ag}},\mathrm{R_s})}\sin(n\theta+\psi_n) \end{aligned} \tag{15}$$

III. Transfer of Surface Forces in Single Magnetic Wave Case

This section aims to compare the airgap surface forces (4) calculated at radius $\mathrm{R_{ag}}$ with the exact value calculated at $\mathrm{R_s}$. Then an airgap surface radial force function is defined:

$$P_{\mathrm{r}} : \begin{cases} [\mathrm{R_{ag}},\mathrm{R_s}]\times[0,2\pi] & \rightarrow & \mathbb{R} \\ (r,\theta) & \rightarrow & \frac{1}{2\mu_0}\left(B_{\mathrm{r}}^2(r,\theta) - B_{\theta}^2(r,\theta)\right) \end{cases} \tag{16}$$

In order to better understand the airgap transfer of the forces, a Fourier decomposition is performed:

$$P_{\mathrm{r}}(r,\theta) = P_{r,0}(r) + P_{r,2n}(r)\cos(2n\theta+2\psi_n) \tag{17}$$

The previous result (15) allows to express the magnetic flux under the form:

$$\begin{aligned} B_r(r,\theta) &= B_{r,n}(r)\cos(n\theta+\psi_n) \\ B_\theta(r,\theta) &= B_{\theta,n}(r)\sin(n\theta+\psi_n) \end{aligned} \tag{18}$$

Then the airgap radial surface force can be decomposed under the form:

$$\begin{aligned} P_{r,0}(r) &= \left(B_{r,n}^2(r) - B_{\theta,n}^2(r)\right)/2 \\ P_{r,2n}(r) &= \left(B_{r,n}^2(r) + B_{\theta,n}^2(r)\right)/2 \end{aligned} \tag{19}$$

This is a classical result: a magnetic wavenumber n in the airgap is recomposed into magnetic force wavenumbers 0 and $2n$. For the studied slotless case $\forall\theta\in[0,2\pi]$, $B_\theta(\mathrm{R_s},\theta) = 0$. In order to avoid θ dependency, the amplitude of each harmonics are compared independently. To this purpose, a function is defined $\forall r\in[\mathrm{R_{ag}},\mathrm{R_s}]$, for $k\in\mathbb{N}$:

$$R_k(r) = P_{r,k}(r)/P_{r,k}(\mathrm{R_s}) \tag{20}$$

The next step is to introduce the analytic solution of the magnetic flux (15) into (20) in order to get the analytic expression of each function R_0 and R_{2n}. After some calculations, the expression of these two functions simplify remarkably well as follows for $k=0$ or $k=2n$:

$$R_k(r) = \left(\mathrm{R_s}/r\right)^2 F_k(r,\mathrm{R_s})/2 \tag{21}$$

Note that $\forall r$, $F_0(r,\mathrm{R_s}) = 1$. Then combining (17) with (21), the relation between the airgap radial surface force and the exact radial surface force at position $r=\mathrm{R_s}$ can be established:

$$P_{\mathrm{r}}(\mathrm{R_s},\theta) = \frac{r^2}{\mathrm{R_s^2}}\left(P_{r,0}(r) + \frac{2P_{r,2n}(r)}{F_{2n}(r,\mathrm{R_s})}\cos(2n\theta+2\psi_n)\right) \tag{22}$$

The differences between exact radial surface force density and airgap radial surface force depends on the airgap width, the radius of application and the wavenumber, but not on the magnetic excitation β_n. If the airgap surface forces are equivalent to the exact surface forces at $\mathrm{R_s}$, then both R_0 and R_{2n} should be very close to 1 for every wavenumbers and for any radius. Fig. 2 shows that these coefficients are not always negligible and they can strongly affect high magnetic surface force wavenumbers. Nevertheless, the vibro-acoustic of electrical machine generally considers only low wavenumbers such that the airgap surface force stays relatively accurate in the radial direction with narrow airgaps. A similar method is applied to estimate the impact of the airgap transfer on the tangential surface force, with the following function:

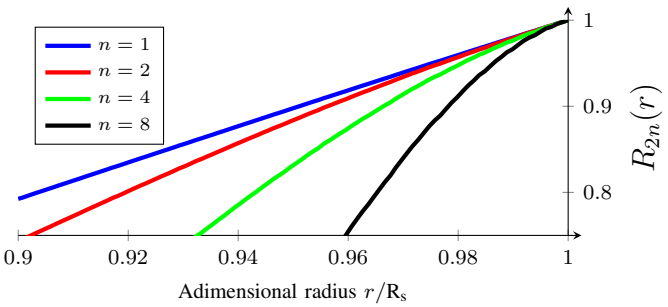

Fig. 2. Comparing stator and airgap Maxwell Tensor magnetic surface force for the harmonic $2n$

$$P_{\theta} : \begin{cases} [\mathrm{R_{ag}},\mathrm{R_s}]\times[0,2\pi] & \rightarrow & \mathbb{R} \\ (r,\theta) & \rightarrow & \frac{1}{\mu_0}B_{\mathrm{r}}(r,\theta)B_{\theta}(r,\theta) \end{cases} \tag{23}$$

Then the next result can be easily demonstrated following the same methodology:

$$P_{\theta}(r,\theta) = -\frac{\mathrm{R_s^2}}{r^2}\frac{E_{2n}(r,\mathrm{R_s})}{2}P_{r,2n}(\mathrm{R_s})\sin(2n\theta+2\psi_n) \tag{24}$$

In order to estimate the relative error Δ, the airgap width is defined as g with $g = 2\left(\mathrm{R_{ag}} - \mathrm{R_s}\right) \ll \mathrm{R_{ag}}$. Then a Taylor approximation on (24) leads to:

$$\Delta \propto 2ng/\mathrm{R_{ag}} \tag{25}$$

However on the studied case, the tangential surface force density should be null. A new criterion can be defined: $\Delta \ll 1$ means that airgap surface forces are accurate. Note that the resultant torque is constant for any radius - $\int_0^{2\pi} P_\theta(r,\theta)r\mathrm{d}\theta$ = 0 - but it is not true for the total radial force because it is varying linearly with the radius of application: $\int P_{\mathrm{r}}(r,\theta)\mathrm{d}\theta = \frac{\mathrm{R_s}}{r}\int P_{\mathrm{r}}(\mathrm{R_s},\theta)\mathrm{d}\theta$. Nevertheless, the transfer coefficient does not change the unbalanced magnetic forces F_x and F_y in the Cartesian referential.

IV. Generalization to Multi-Harmonic Case

The previous section demonstrates a new transfer coefficient for single magnetic excitation wave. In this section, the coefficient (21) is validated to any combination of wavenumbers.

$\hat{P}_{\mathrm{r}}$ is the Fourier transform of P_{r} and if $\hat{P}(r,k)$ is the k^{th} harmonic of the airgap surface force (4) :

$$P_{\mathrm{r}}(r,\theta) = \sum_k \hat{P}(r,k)\cos(k\theta+\phi_k) \tag{26}$$

From this airgap surface force, a transfer model is proposed by assuming that - despite the recombination of several flux

TABLE I
INJECTED MAGNETIC POTENTIAL SPECTRUM FOR THE VALIDATION CASE WITH $R_{AG} = 42.5\,mm$ AND $R_S = 45.0\,mm$.

Wavenumber n	5	7	15	17	19
Amplitude β_n [T.m]	5.2615	0.6861	0.2119	0.2725	0.1926
Phase ψ_n [rad]	3.8893	0.7100	0.4700	0.6849	0.5410

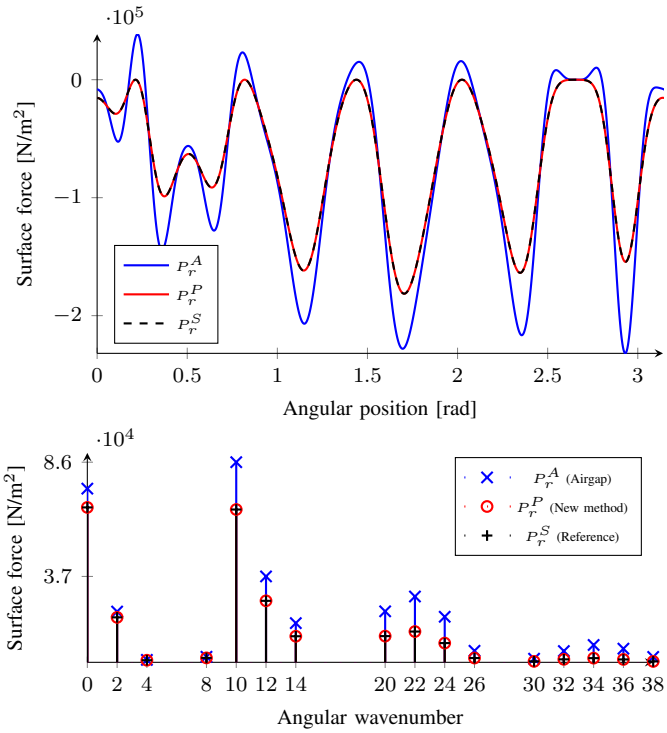

Fig. 3. Comparison of several methods for surface force density using Maxwell Tensor

density harmonics into one force harmonic - the coefficient (21) stays valid:

$$P_{\mathrm{r}}(\mathrm{R_s},\theta) = \sum_k \frac{2\hat{P}(r,k)}{F_k(r,\mathrm{R_s})}\cos(k\theta+\phi_k) \tag{27}$$

The validity of the assumption is verified for the same slotless case as in Fig. 1 with infinite ferromagnetic permeability. Thus the flux density is entirely solved analytically using a linear combination of (15). The numerical inputs of the validation case are presented in Table I. The results are presented in Fig. 3: P_{r}^A denotes the application of (16) at $r = \mathrm{R_{ag}}$, P_{r}^P denotes the application of (27), and P_{r}^S denotes the exact value of magnetic surface forces obtained with (16) at $r = \mathrm{R_s}$. Comparing the L^2-norm of the two signals with respect to the stator surface forces leads to:

$$\|P_{\mathrm{r}}^{\mathrm{P}} - P_{\mathrm{r}}^{\mathrm{S}}\|_{L^2} \approx 10^{-5}\|P_{\mathrm{r}}^{\mathrm{A}} - P_{\mathrm{r}}^{\mathrm{S}}\|_{L^2} \tag{28}$$

A perfect match is observed between the $P_{\mathrm{r}}^{\mathrm{P}}$ and the $P_{\mathrm{r}}^{\mathrm{S}}$, which means that the intuited formula (27) is correct at least for the slotless geometry. A similar result can be found with the tangential component.

This last result allows the partial use of these coefficients for slotted electrical machine: all the previous results hold when the angular domain is restricted. Thus supposing the previous reasoning is applied on the angular opening of an electrical machine stator's tooth tip - with infinite ferromagnetic permeability - then the transfer method (27) can be applied but only for this restricted angular opening. Nevertheless, the transfer of the airgap surface force based on MT in front of the slotted area might not be properly predicted with these coefficients.

V. CONCLUSION

This paper objective was to understand to what extent the surface force density computed at the airgap radius with Maxwell Tensor differs from the exact magnetic force density. For this purpose, a simplified slotless academic machine was defined in order to find analytical surface force transfer coefficients. The study of a single flux density excitation demonstrates the existence of a a new transfer coefficient. The final part of the paper shows that these transfer coefficients remain unchanged with a multi-harmonic magnetic excitation.

The importance of these transfer coefficients depends on the airgap size and force wavenumbers to be taken into account for vibroacoustic analysis. Only these two factors were identified. The transfer coefficients have little influence on low magnetic force wavenumbers but significant influence on high force wavenumbers. Consequently, these coefficients can be used to estimate the deviation between the surface force calculated in the air and the surface force calculated on the stator bore radius. Considering infinite permeability, the transfer coefficients could be applied to correct the radial magnetic surface forces from the airgap Maxwell Tensor with a real electrical machine, but only in front of a tooth tip.

Future research work will address the generalization of these coefficients to slotted areas of electrical machines and to tangential surface forces. The authors expect to use this slotless machine as a reference case in future development of magneto-mechanical coupling methods: the simplified geometry allows to solve analytically the magnetic and mechanical equations such that it could be compared to numerical and experimental results in future research work.

REFERENCES

[1] J. F. Gieras, C. Wang, and J. C. Lai, *Noise of polyphase electric motors*. CRC Press, 2005.

[2] X. Xu, Q. Han, and F. Chu, "Review of electromagnetic vibration in electrical machines," *Energies*, vol. 11, no. 7, 2018.

[3] F. Henrotte and K. Hameyer, "Computation of electromagnetic force densities: Maxwell stress tensor vs. virtual work principle," *J. Comput. Appl. Math.*, vol. 168, no. 1-2, pp. 235–243, 2004.

[4] J. Mizia, K. Adamiak, A. Eastham, and G. Dawson, "Finite element force calculation: comparison of methods for electric machines," *IEEE Trans. Magn.*, vol. 24, no. 1, pp. 447–450, 1988.

[5] Z. Ren, "Comparison of Different Force Calculation Methods in 3D Finite Element Modelling," *IEEE Trans. Magn.*, vol. 30, no. 5, pp. 3471–3474, 1994.

[6] J. Hallal, F. Druesne, and V. Lanfranchi, "Study of electromagnetic forces computation methods for machine vibration estimation," in *ISEF Conference*, 2013, pp. 12–14.

[7] R. E. Rosensweig, *Ferrohydrodynamics*. Cambridge University Press, 1985.

[8] L. D. Landau and E. Lifshitz, "The classical theory of fields. vol. 2," *Course of theoretical physics*, 1975.

[9] T. Lubin, S. Mezani, and A. Rezzoug, "Exact analytical method for magnetic field computation in the air gap of cylindrical electrical machines considering slotting effects," *IEEE Trans. Magn.*, vol. 46, no. 4, pp. 1092–1099, 2010.